geosciences

MDPI

Article

Modeling Thermal Conductivity of Sandy Soils Under Unfrozen Temperature Conditions

Aashish Pokhrel, Laureano R. Hoyos and Xinbao Yu *

Department of Civil Engineering, University of Texas, Arlington, TX 76019, USA; axp8401@mavs.uta.edu (A.P.); hoyos@uta.edu (L.R.H.)
* Correspondence: xinbao@uta.edu

Abstract

Soil thermal conductivity is a key parameter in modeling heat transfer, temperature-driven moisture migration, artificial ground freezing, and geothermal systems. However, most existing thermal-conductivity models do not account for temperature effects. This study aims to determine the temperature-dependent thermal conductivity of silty and fine sandy soils at elevated temperatures using a steady-state heat cell method, addressing the limitations of transient probe techniques, which are affected by air voids and heat loss at the needle–soil interface. The experiment employs a heat cell under one-dimensional steady-state heat-transfer conditions, with sufficiently small temperature gradients to prevent temperature-induced moisture migration, and measures the soil's thermal properties at steady state by indirect temperature and heat-flux measurements using various sensors. The test observations showed well-correlated thermal conductivity readings from steady state and transient probe methods at room temperature. Furthermore, the measured thermal conductivity of the sandy soil demonstrated a near-linear increase with temperature, with the highest dependence at 15.1% and 22.5% saturation for Benbrook (SM) and fine-grained Ottawa (SP) sands, respectively. Several commonly used existing thermal conductivity models were used to fit the measured thermal conductivity. A new thermal conductivity model was developed, incorporating a temperature-dependent correction based on the best-fit model. The proposed model could more accurately capture the increased thermal conductivity of soils with temperature. The findings will significantly improve the modeling of soil-temperature-dependent multi-physics behavior.

Keywords: thermal conductivity; thermal conductivity function; temperature; unsaturated soil

Check for updates

Academic Editors: Chencong Liao and Evgeny Chuvilin

Received: 26 December 2025
Revised: 10 April 2026
Accepted: 22 April 2026
Published: 27 April 2026

Copyright: © 2026 by the authors. Licensee MDPI, Basel, Switzerland. This article is an open access article distributed under the terms and conditions of the Creative Commons Attribution (CC BY) license.

1. Introduction

Heat transfer in soils plays an important role in several geotechnical and agricultural activities, including seed germination and plant growth [1], evaluation of the frost penetration depth [2], studies of the coupled heat and moisture transfer in soils [3], efficient designs of geothermal heat exchangers [4], and prediction and evaluation of the effect of free-thaw cycles in soils [5]. Heat transfer in soil occurs primarily by conduction and convection, while radiative heat transfer is negligible. The contribution of convective heat transfer in fine sandy soils under closed unsaturated systems is found to be negligible due to the small unsaturated permeability of the soil [6,7]. Thus, heat transfer in soil mainly occurs through conduction and diffusion, with the soil's thermal conductivity being a primary parameter controlling the rate of heat transfer.

Thermal conductivity of soils is primarily measured using the transient probe method, which applies a constant-current pulse for a short period and records the soil's response to heating at different radial distances [8,9]. The quick, easy operation of the transient probes allows for measurement within an hour using a prefabricated thermal probe [10]. However, the entrapped air bubbles at the interface impede heat transfer from the thermal conductivity needles to the soil, which usually leads to an underestimation of the thermal conductivity [11,12]. Although the use of thermal greases has been suggested, the effect of greases on the thermal conductivity measurement of soils has yet to be studied [13]. The melting of ice during transient heating in frozen soils has been observed, often leading to erroneous thermal conductivity readings [14]. Thus, although more tedious, the steady-state method can yield more accurate measurements by eliminating the limitations inherent in the transient probe method.

The use of thermal conductivity functions (TCFs) has become increasingly widespread as numerical modeling of geothermal applications has increased. However, the thermal conductivity of the soils depends on various factors, including saturation, dry density, mineralogy, gradation, textures, and temperature [13]. The thermal conductivity modeling of the soils can be a challenging task because of microstructures, connectivity of the phases, and their interactions [15]. Numerous empirical, mathematical, physics-based, and combined TCFs have been developed for different soil types, and the search for a better model is still ongoing [16–18].

The earliest TCF includes Kersten [19] thermal conductivity model based on different empirical formulas for sands, silts, and clays. It is one of the simplest models and is still commonly used for thermal conductivity evaluation, in which the empirical parameters are determined based on saturation. Later, Campbell [20] developed a five-parameter model, which is difficult to implement in the wide range of soils due to the high number of parameters. Numerous current studies have improved the Kersten TCF by including more parameters to model the thermal conductivity for varying soil conditions, and also extending it to frozen soils [21,22].

Furthermore, the physically modeled TCFs have been developed to predict thermal conductivities across a wide range of soil types and conditions. One of the earliest and still most common models includes the De Vries model [7], which considers the volume fraction of different phases to evaluate the effective thermal conductivity of the mixture. De Vries TCF captures the overall trend in thermal conductivity; however, it lacks the non-linear variation in thermal conductivity with saturation. Tarnawski et al. [23] furthered De Vries model by introducing soil mineralogy into the formulation. Moreover, geometric and harmonic mean models have also been used, mostly to create more complex TCFs rather than for standalone model formulation.

The physically developed models are improved with empirical parameters to formulate more accurate TCFs that also capture the non-linear trend in thermal conductivity. Johansen's [24] model is one of the oldest and most common models that improved Kersten's [19] model by introducing a parameter linking the Kersten number to the saturation ratio. Côté and Konrad [25] further improved the model by using more empirical parameters based on the soil gradation and saturation ratio. Lu et al. [21] introduced an exponential and power-law-based empirical formula to evaluate the Kersten number. Liu et al. [26] further improved the model by introducing the Soil Water Characteristics Curve (SWCC) based empirical formulation based on Bi et al.'s [27] model. Cao et al. [28] later introduced the temperature effect on the SWCC-based model for the thermal conductivity prediction, but the complexity of the model, along with the requirement of van Genuchten SWCC parameters, makes it difficult to apply in general soils. Lately, Ji et al. [29] extended Ghanbarian and Daigle's [30] general effective medium (GEM) framework to

a unified model that works in both frozen and unfrozen soils by the introduction of an unfrozen water content parameter, but still lacks the introduction of the proper temperature effect on the thawed soils under elevated temperature. Furthermore, the progress in machine learning (ML) has led to several model developments with temperature, saturation, dry density, porosity, mineralogy, etc., as independent variables [31,32]. However, the 'black box' nature of these models does not allow easy implementation in finite element software and general data analysis.

Significant research has been conducted on the development of thermal conductivity functions (TCFs), with emphasis on various soil properties as predictive variables. However, the effect of temperature on the thermal conductivity of unsaturated soils has been modeled either using simplified approaches that fail to capture observed trends or through sophisticated machine-learning and SWCC-based models that are difficult to implement in finite-element (FE) software. Furthermore, the near-linear dependence of thermal conductivity on temperature in unsaturated soils has not been widely reported, leading to a lack of temperature-dependent TCFs that can be applied within simpler modeling frameworks. This study developed a heat cell to measure the thermal conductivity of sandy soils at various temperatures. The measured thermal conductivity datasets were used to evaluate the performance of commonly used thermal conductivity models when temperature is treated as a variable. In addition, a simplified thermal conductivity model is proposed by extending the formulation of Lu et al. [21] to incorporate the effect of temperature on the thermal conductivity of sandy soils.

2. Methods and Materials

2.1. Soil Heating Cell

The heating cell consists of two concentric acrylic cylinders, each 0.635 cm (0.25 in) thick, with internal diameters of 8.89 cm (3.5 in) and 20.96 cm (8.25 in), and a height of 10.16 cm (4 in), as shown in Figure 1. The cylinders are secured in position by top and bottom heat exchanger systems, each comprising a copper plate adjacent to the soil specimen and an acrylic plate with water circulation channels on the exposed side. The heat exchanger plate with spiral water channels, along with the temperature-controlled fluid circulator, is presented in Figure 2. Two heat flux sensors (FHF05SC, Hukseflux, Center Moriches, NY, USA) were installed to measure heat flux, accompanied by three T-type thermocouples to monitor soil temperature and calculate temperature gradients, as shown in Figure 3. A moisture sensor (EC-5, METER Group, Pullman, WA, USA) was used to detect any moisture fluctuations during the heating tests. Two temperature-controlled water baths (PolyScience, Niles, IL, USA) regulated the heat exchanger temperature within ± 0.04 °C of the target value. Measurements were obtained from the inner soil specimen, while the outer cylinder was compacted to the same degree to serve as a buffer and provide additional insulation. Furthermore, fiberglass insulation was installed around the device to minimize radial heat transfer and prevent heat loss.

2.2. Soils

Fine and silty sands were primarily used for experimental study. Two fine-grained Ottawa sands, namely ASTM C778 and ASTM 50–70 from Humboldt Mfg. Co, Elgin, IL, USA, and Silty sand from Benbrook, TX, USA, at different saturations were used for the heating test. These Ottawa sands contain uniformly graded ASTM 50–70 sand with sand particles confined between ASTM No. 50 and 70 sieves and C778 with poorly graded fine sand retained between sieve No. 20 and 100 sieves. The fine-grained sands were classified as poorly graded sand (SP), and the Benbrook sand was classified as silty sand (SM) with

non-plastic fines based on the Unified Soil Classification System (USCS). The gradation of the soil used for the laboratory tests is presented in Figure 4.

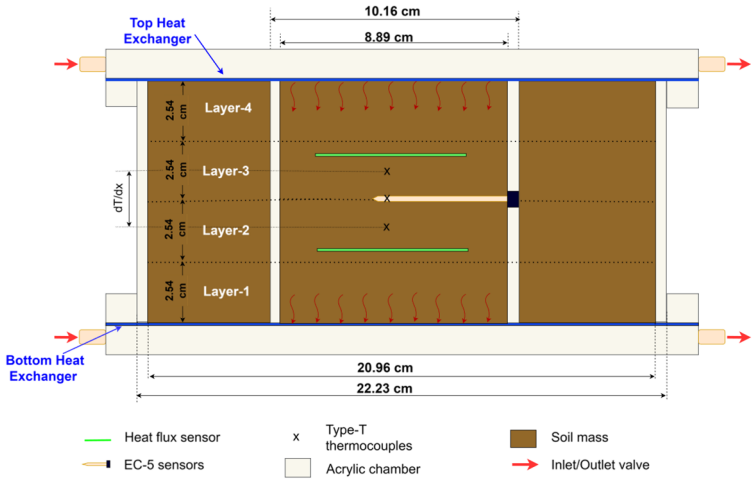


Figure 1. Schematic diagram of the heating cell with approximate sensor locations. The wavy arrows indicate the imposed heat flow direction.

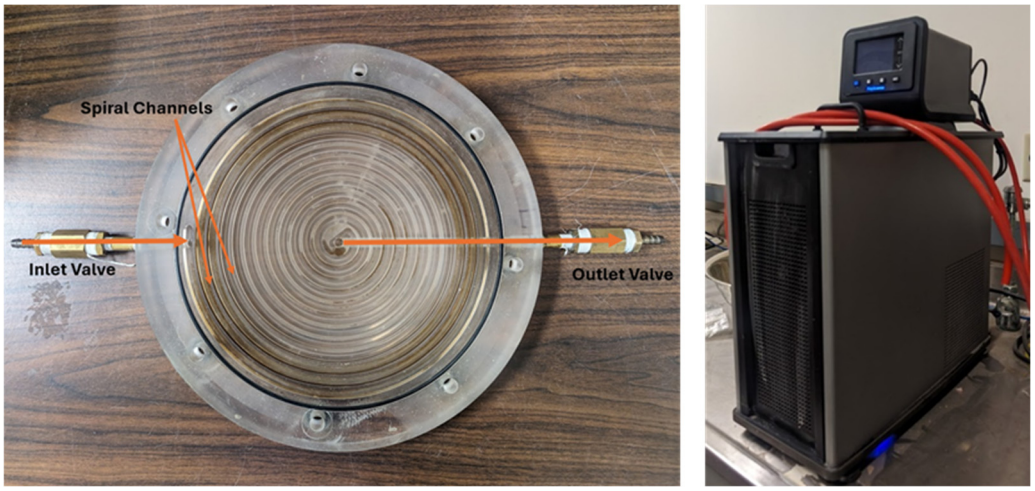


Figure 2. Top heat exchanger disk with spiral grooves (**left**) and temperature-controlled bath circulator (**right**).

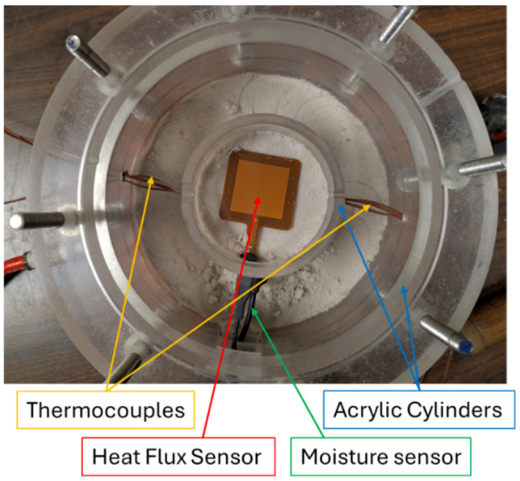


Figure 3. Picture showing the compacted sand with different embedded sensors.

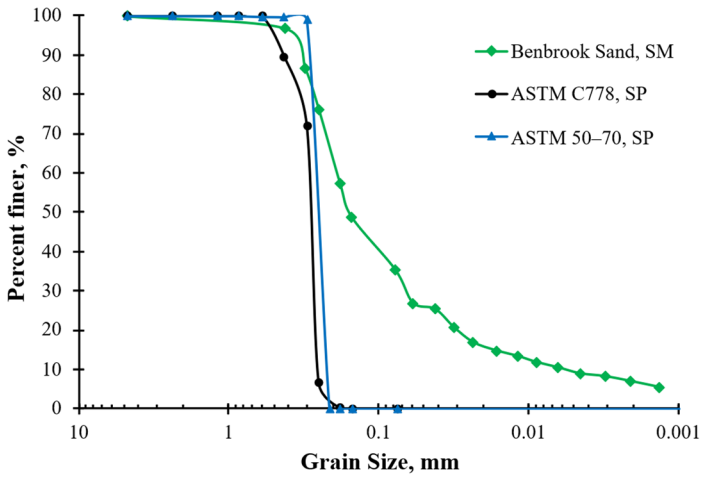


Figure 4. Gradation curve of the three soils used for thermal conductivity measurement.

2.3. Methodology

The preparation of the standard soil specimen included oven drying of the soil at 105 °C for 24 h before pulverizing and mixing it with deionized water to reach the desired saturation. The samples were allowed to sit in a closed container for at least 24 h in a humidity-controlled room to facilitate the moisture equilibrium within the soil before soil compaction in the heating cell. The measured quantity of the soil was then compacted to reach a near 1.6 g/cm^3 dry density by dynamic compaction with gentle tamping in four layers. The initial soil properties after compaction are presented in Table 1. The sensors were installed at their specific locations during the soil compaction. The sensor installation ports in the acrylic cylinders were sealed with silicon putty, followed by duct tape to inhibit the moisture loss from the system. The entire system was covered with fiberglass insulation on all sides to ensure the one-dimensional steady-state heat flow through the soil specimen.

Table 1. Table showing the soil properties after compaction.

Soil Type	Moisture Content		Dry Density	Porosity, n
	Gravimetric, %	Volumetric, -	g/cm^3	
Benbrook Sand (SM)	0.99	0.016	1.596	0.40
	4.99	0.077	1.546	0.46
	7.00	0.098	1.412	0.43
	10.61	0.163	1.533	0.42
	11.85	0.180	1.521	0.43
	12.79	0.219	1.570	0.41
ASTM C778 (SP)	0.20	0.003	1.614	0.39
	5.17	0.080	1.538	0.42
	9.27	0.146	1.574	0.41
ASTM 50–70 (SP)	0.10	0.002	1.655	0.38
	8.75	0.134	1.534	0.42
	10.40	0.189	1.555	0.41

The system was heated on one side and cooled on the other to maintain a temperature gradient of less than 3 °C, leading to a thermal gradient of less than 30 °C/m to prevent moisture migration during the heating test. This was also monitored by the installed

moisture sensor. The heating continued until the soil specimen reached a steady state, which was indicated by the temperature change of less than 0.1 °C and the heat flux of less than 0.5 W/m^2 within an hour. The system was allowed to run for one more hour, during which the data was collected for the thermal conductivity calculation. The heating direction was switched at each subsequent temperature increment to offset possible moisture migration driven by the temperature gradient.

3. Thermal Conductivity Measurement

The heating cell delivered the lateral steady-state heat flux through the cylindrical soil specimen. Two heat flux sensors placed within the soil specimens measured the steady heat flux through the soil specimen (W/m^2). The thermocouples placed at different positions in the inner soil specimens aided in the calculation of the temperature gradient and the average temperature of the soil specimen, as shown in Figure 5. Based on the average heat flux through the system and the calculated temperature gradient, the effective thermal conductivity of the soil specimen can be calculated using Equation (1), where the negative symbol signifies the heat flow from high to low temperature. The temperature gradient at the thermal conductivity measurement point can be calculated by using Equation (2).

$$k_{eff} = -q/(\partial T/\partial x) \quad (1)$$

q: heat flux (W/m^2), k_{eff}: effective thermal conductivity of soil, $\partial T/\partial x$: temperature gradient (°C/m).

$$\partial T/\partial x = (T_1 - T_3)/\Delta x \quad (2)$$

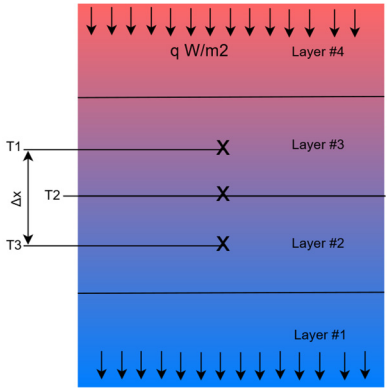


Figure 5. The schematic shows the locations of the thermocouples used to measure the temperature gradient and the average temperature of the soil specimen. The arrows represent the direction of applied heat flux through the specimen.

4. Verification of the Heating Cell

The thermal conductivity of the soil specimen was measured at multiple locations using the transient probe method with a TR-1 sensor (Meter Group, Pullman, WA, USA) immediately after specimen preparation in the heating cell. The same soil specimen was used to measure thermal conductivity using the steady-state method with a heating cell. Figure 6 compares the thermal conductivity readings from the transient probe at the room temperature with the measured thermal conductivity from the steady-state method.

The thermal conductivity measured from the heating cell using the steady-state method closely aligns with the measurements made from the transient probe method, with $R^2 = 0.977$. The transient probe method yields slightly lower thermal conductivity values at room temperature, likely due to heat loss associated with air voids at the soil–sensor interface. This error could not be mitigated because consistent measurements

from both methods across a wide range of temperatures and moisture levels were required. Moreover, the heating tests were conducted over a broad temperature range, including temperatures close to freezing, where errors associated with the transient probe method tend to increase. This further supports the steady-state method as the more suitable approach in these temperature ranges.

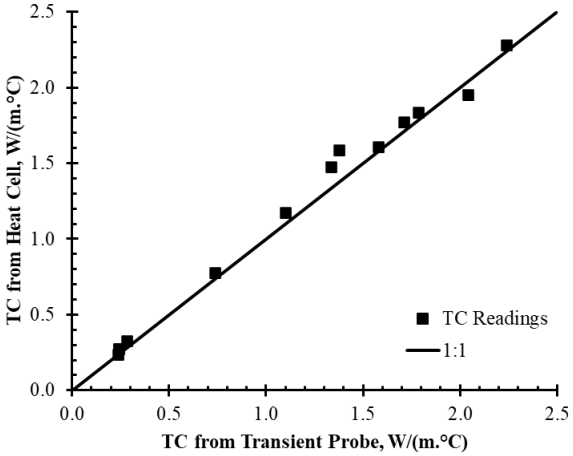


Figure 6. Comparative thermal conductivity from a heat cell using the steady-state method and a transient probe at room temperature.

5. Thermal Conductivity Models

Among the numerous TCFs available, the most common thermal conductivity models were used for data analysis. Empirical, mathematical, and combined models were used to evaluate how past TCFs performed relative to the proposed one. However, the SWCC-based models were not used in the analysis due to the greater number of required parameters and the unknown SWCC parameters of the test soils. Additionally, for the temperature-based thermal conductivity evaluation, the thermal conductivity of each phase, solids and fluids, was changed with temperature in the respective TCFs whenever pertinent.

5.1. Thermal Conductivity of the Materials

The thermal conductivity of different components, solids, and fluids is highly dependent on the temperature. The thermal conductivity of the silica (SiO_2) drops with the temperature, whereas the thermal conductivity of the pore fluids increases with temperature [33]. The Ottawa sand consisted of silica sand, for which the thermal conductivity of the solids was assumed based on the dataset from Powell et al. [33] in the 0 °C to 70 °C temperature with Equation (3).

$$\lambda_q = 9.1552 - 0.0278T\ [^\circ C] \quad (3)$$

However, Benbrook sand also consists of fine-grained soil. The proportion retained on No. 75 sieve (0.075 mm) is assumed to consist of silica sand and the finer portions as Kaolinite. Since the temperature effect on the Kaolinite solids is unknown, constant thermal conductivity is assumed based on the method of Midttømme et al. [34]. The resulting thermal conductivity of the solids, thus, can be written based on the volumetric mixing formulation of Johansen [24] as given in Equation (4).

$$\lambda_s = \lambda_q^{f_q} \lambda_c^{1-f_q} \quad (4)$$

The thermal conductivity of the water was taken from the Engineering Toolbox [35] dataset, and can be approximated ($R^2 = 0.976$) in 0 °C to 70 °C temperature range with Equation (5).

$$\lambda_w = 0.5646 + 0.0015T\ [^\circ C] \quad (5)$$

λ_s : thermal conductivity of solids, $\lambda_q, \lambda_c, \lambda_w$: thermal conductivity of quartz, clay, and water, f_q: volume fraction of quartz.

5.2. Johansen Model

Johansen [24] modified Kersten [19] thermal conductivity model by updating the Kersten number (K_e) based on the different logarithmic relations with saturation for coarse- and fine-grained soils, which are given in Equations (6)–(9). The upper limit or the saturated thermal conductivity (λ_{sat}) is evaluated based on the volumetric mixing formula with porosity of the soil as the determining parameter. However, the lower limit for thermal conductivity (λ_{dry}) is determined based on the dry density of the soil.

$$\lambda_{eff} = K_e\left(\lambda_{sat} - \lambda_{dry}\right) + \lambda_{dry} \quad (6)$$

$$K_e = \begin{cases} 0.7\log(S_r) + 1 & \text{for } S_r > 0.05, \text{ coarse soil} \\ \log(S_r) + 1 & \text{for } S_r > 0.1, \text{ fine soil} \end{cases} \quad (7)$$

$$\lambda_{sat} = \lambda_W^P \cdot \lambda_s^{1-P} \quad (8)$$

$$\lambda_{dry} = \frac{0.135\rho_d + 0.0647}{\rho_s - 0.947\rho_b} \quad (9)$$

λ_{eff} : effective thermal conductivity of soil, K_e : Kersten number, λ_{sat} : saturated thermal conductivity of soil, λ_{dry} : thermal conductivity of dry soil, P : porosity, ρ_d : dry density, ρ_b : bulk density, ρ_s : density of the solids, S_r : saturation ratio.

5.3. Côté and Kondrad [25] Model

Côté and Konrad [25] introduced an empirical parameter k_1 that allows the non-linear variation in the Kersten number (K_e) with saturation of the soil based on the hyperbolic dependencies between them as presented in Equations (10)–(13). This model further uses a power equation to estimate the soil's dry thermal conductivity, with the help of two additional empirical parameters and a power function. This model was further extended by Liu et al. [26] to introduce the thermal conductivity under freezing conditions.

$$\lambda_{eff} = K_e\left(\lambda_{sat} - \lambda_{dry}\right) + \lambda_{dry} \quad (10)$$

$$K_e = \frac{k_1}{1 + (k_1 - 1)\cdot S_r} \quad (11)$$

$$\lambda_{dry} = \chi 10^{-n,\eta} \quad (12)$$

$$\lambda_{sat} = \lambda_s^{1-n} \cdot \lambda_w^n \quad (13)$$

$k_1\eta, \chi$: constitutive parameters, n : porosity, λ_s: thermal conductivity of solids, λ_w: thermal conductivity of water.

5.4. Campbell et al. [20] Model

Campbell et al. [20] modified the mathematical model proposed by formula De Vries [36] by introducing the adjustable shape factors along with the influence factor of the saturation. The model calculates the influence of all phases, solids, water, and air, based on the equivalent thermal conductivity of the pore fluids, which is dependent on

the temperature. The final thermal conductivity from the Campbell et al. model can be determined by using Equations (14)–(20).

$$\lambda = \left[\frac{k_w x_w \lambda_w + k_a x_a \lambda_a + k_m x_m \lambda_m}{k_w x_w + k_a x_a + k_m x_m}\right] \tag{14}$$

$$k_a = \frac{1}{3}\left[\frac{2}{1+\left(\frac{\lambda_a}{\lambda_f}-1\right)g_a} + \frac{1}{1+\left(\frac{\lambda_a}{\lambda_f}-1\right)g_c}\right] \tag{15}$$

$$k_w = \frac{1}{3}\left[\frac{2}{1+\left(\frac{\lambda_w}{\lambda_f}-1\right)g_a} + \frac{1}{1+\left(\frac{\lambda_w}{\lambda_f}-1\right)g_c}\right] \tag{16}$$

$$k_m = \frac{1}{3}\left[\frac{2}{1+\left(\frac{\lambda_m}{\lambda_f}-1\right)g_a} + \frac{1}{1+\left(\frac{\lambda_m}{\lambda_f}-1\right)g_c}\right] \tag{17}$$

$$\lambda_f = \lambda_a + f_w(\lambda_w - \lambda_a) \tag{18}$$

$$f_w = \frac{1}{1+(x_w/x_{wo})^{-q}} \tag{19}$$

$$q = q_o\left(\frac{\Theta}{303}\right)^2 \tag{20}$$

x_w, x_a, x_m : volume fractions of water, air, and solids, $\lambda_w, \lambda_a, \lambda_m$: thermal conductivities of three phases, λ_f: effective fluid thermal conductivity, f_w: empirical weighing function, x_{wo}, q: parameters linking the water content, which sharply affects the thermal conductivity of the soils, q_o: empirical parameter, Θ: soil temperature in Kelvin, g_a, g_b, g_c: shape factors with $g_a = g_b$ and $g_c = 1 - 2$. g_a, k_w, k_a, k_m : weighing factors for different phases.

5.5. Chen [37] Model

Chen [37] introduced a thermal conductivity model based on the mixing formula and two empirical parameters based on the linear relation between porosity and the logarithm of the dry thermal conductivity. The thermal conductivity function, shown in Equation (21), uses a power function based on the saturation of the soil to introduce nonlinearity with the saturation of the soil.

$$k_{eff} = k_s^{1-n} \cdot k_w^n \cdot n \cdot [(1-b)S + b]^{cn} \tag{21}$$

k_{eff} : effective thermal conductivity of soils, k_s, k_w: thermal conductivity of solids and water, n: porosity, S: saturation, b, c: empirical parameters.

5.6. Lu et al. [21] Model

Lu et al. [21] modified the Johansen [24] model by introducing an exponential-based Kersten number (K_e) with an empirical parameter α as presented in Equation (22). Furthermore, Lu et al. have introduced two empirical parameters based on the dry density of the soil, assuming a linear relation between dry density and porosity of the soil while using the volumetric mixing formula to determine the saturated thermal conductivity of the soil as given in Equations (22) and (24).

$$K_e = \exp\left\{\alpha\left[1 - S_r^{(\alpha-1.33)}\right]\right\} \tag{22}$$

$$\lambda_{dry} = -an + b \tag{23}$$

$$\lambda_{sat} = \lambda_w^n \cdot \lambda_s^{1-n} \tag{24}$$

α : empirical parameter depending on soil texture, S_r: saturation ratio, a, b: empirical parameters, n: porosity.

5.7. Farouki [11] Model

Farouki [11] has modified the Johansen model by changing the Kersten number (K_e) and introducing the thermal conductivity of solids (λ_s) with the arithmetic mean based on the fraction of sands and clays as presented in Equations (25)–(27). The thermal conductivity of the sands and clays is taken as 8.8 W/(m·°C) and 2.2 W/(m·°C), respectively. Furthermore, the Kersten number has been introduced for the freezing condition based on the saturation, but the model fails to consider the temperature effect on the thermal conductivity.

$$\lambda_{eff} = \begin{cases} K_e\left(\lambda_{sat} - \lambda_{dry}\right) + \lambda_{dry} & \text{for } S_r > 10^{-7} \\ \lambda_{dry} & S_r \leq 10^{-7} \end{cases} \quad (25)$$

$$K_e = \begin{cases} \log(S_r) + 1 & \text{for } T \geq T_f \\ S_r & T < T_f \end{cases} \quad (26)$$

$$\lambda_s = \left[8.8f_{sand} + 2.92f_{clay}\right] / \left[f_{sand} + f_{clay}\right] \quad (27)$$

T_f : freezing temperature, f_{sand}: fraction of sand in soil, f_{clay}: fraction of clays in soil.

6. Results

6.1. Thermal Conductivity of the Fine-Grained Sands

The thermal conductivity of both Benbrook and Ottawa sands measured in the lab closely followed a linear increase with temperature at all saturation levels, as shown in Figure 7, where linear best-fit lines have been drawn through the experimental data. The linear best-fit line accurately approximated the thermal conductivity of the sandy soils across all saturation levels. The thermal conductivity of the silty sand showed very little dependence on temperature at near-dry conditions, as indicated by the gentle slope of the thermal conductivity vs. temperature plot in Figure 7. The further increase in saturation led to a greater temperature dependence of the thermal conductivity. However, after a certain saturation, the temperature decreases. The temperature dependence of soil thermal conductivity is described by the slope of the thermal conductivity vs. temperature plot ($\partial k_{eff}/\partial T$) from the experimental dataset. Furthermore, the Ottawa sands showed a higher thermal conductivity at a similar saturation ratio, but the temperature dependency was comparable at a similar saturation.

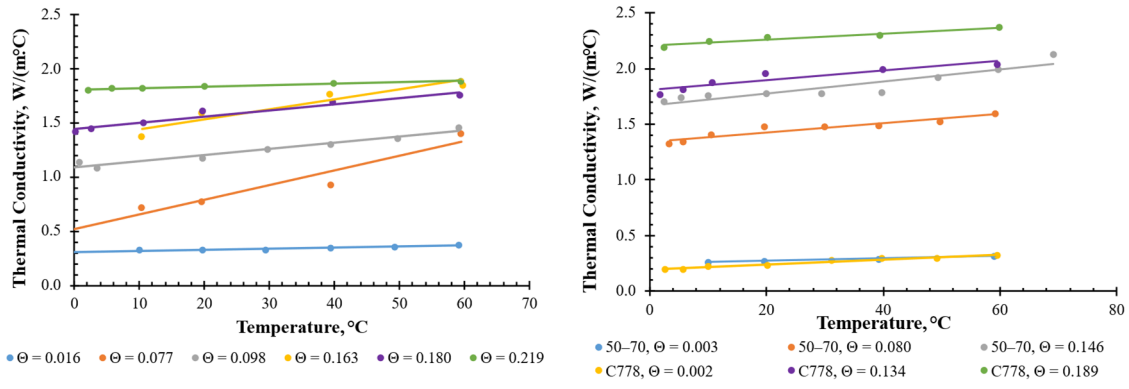


Figure 7. Picture showing the linear fit of thermal conductivity with temperature on the experimental dataset for (**a**) Benbrook sand and (**b**) Ottawa sands.

6.2. Thermal Conductivity Model Assessment

Different thermal-conductivity functions were fitted to the laboratory-test data, including temperature-dependent thermal conductivity for each phase when pertinent. The best-fit models from past thermal conductivity functions for Benbrook sand and Ottawa sands are presented in Figures 8 and 9, respectively. The Farouki [11] model, although one of the oldest, exhibited a satisfactory thermal conductivity at room temperature for Benbrook sand, but it heavily underestimated the thermal conductivity of the Ottawa sands at higher saturations. However, the model failed to capture temperature dependence, yielding nearly constant thermal conductivity readings across all temperature ranges. Johansen [24] model accurately captured the thermal conductivity at the dry state, but heavily underestimated it at higher saturation levels and lacked temperature-dependent modeling for both Benbrook and Ottawa sands. The model proposed by Campbell et al. [20] showed a good fit at the room temperature, but could not capture the temperature dependency of the soils. For the Ottawa sands, the fitted temperature dependency was contradictory to the observed results from the laboratory tests. The greater contribution of solids' thermal conductivity to the effective thermal conductivity led to a decrease in the overall thermal conductivity of the soils. Model proposed by Côté and Konrad [25] and later extended to frozen soil by Liu et al. [26] could fit satisfactory thermal conductivity readings at the room temperature for both silty and fine-grained sands, although it could not model the sharp increase in thermal conductivity of Benbrook (silty) sand from $\theta = 0.077$ to $\theta = 0.098$. The model also failed to account for the temperature dependency of the soil. Chen [37] model fitted the thermal conductivity of the soils at higher saturation for all fine-grained sands; however, it hugely overestimated the thermal conductivity of near-dry soils. The temperature effect also went unnoticed by the Chen model. The model proposed by Lu et al. [21] was able to capture the thermal conductivity of both sands along all saturation levels at room temperature. However, the temperature dependency is still missing from the model, as it yields nearly identical thermal conductivity readings across all temperature ranges.

6.3. Proposed Thermal Conductivity Model

Although various authors have defined several TCFs, they have not been able to capture the temperature dependence of thermal conductivity across various saturations. Thus, to capture this rapidly increasing and gradually declining dependency of thermal conductivity on the temperature with saturation (S), an asymmetric bell-shaped curve defined by an exponential-based function given in Equation (28) is recommended. The equation captures the initial steep increase in thermal conductivity dependency, resulting from the improved particle contact and increased diffusive heat transfer, with temperature ($\partial k_{eff}/\partial T$) and reaches a peak followed by a gradual decline. The parameters A, B, and C control the peak, scaling, and shape of the curve, respectively. These parameters, when fitted to a soil, yield an asymmetric bell-shaped curve that accurately captures the temperature dependence of thermal conductivity at different saturations. The acquisition of this bell-shaped curve requires fitting the thermal conductivity dataset and obtaining the parameters based on the lowest error or the highest coefficient of determination.

$$\partial k_{eff}/\partial T = AS(B - S)e^{-CS} \quad (28)$$

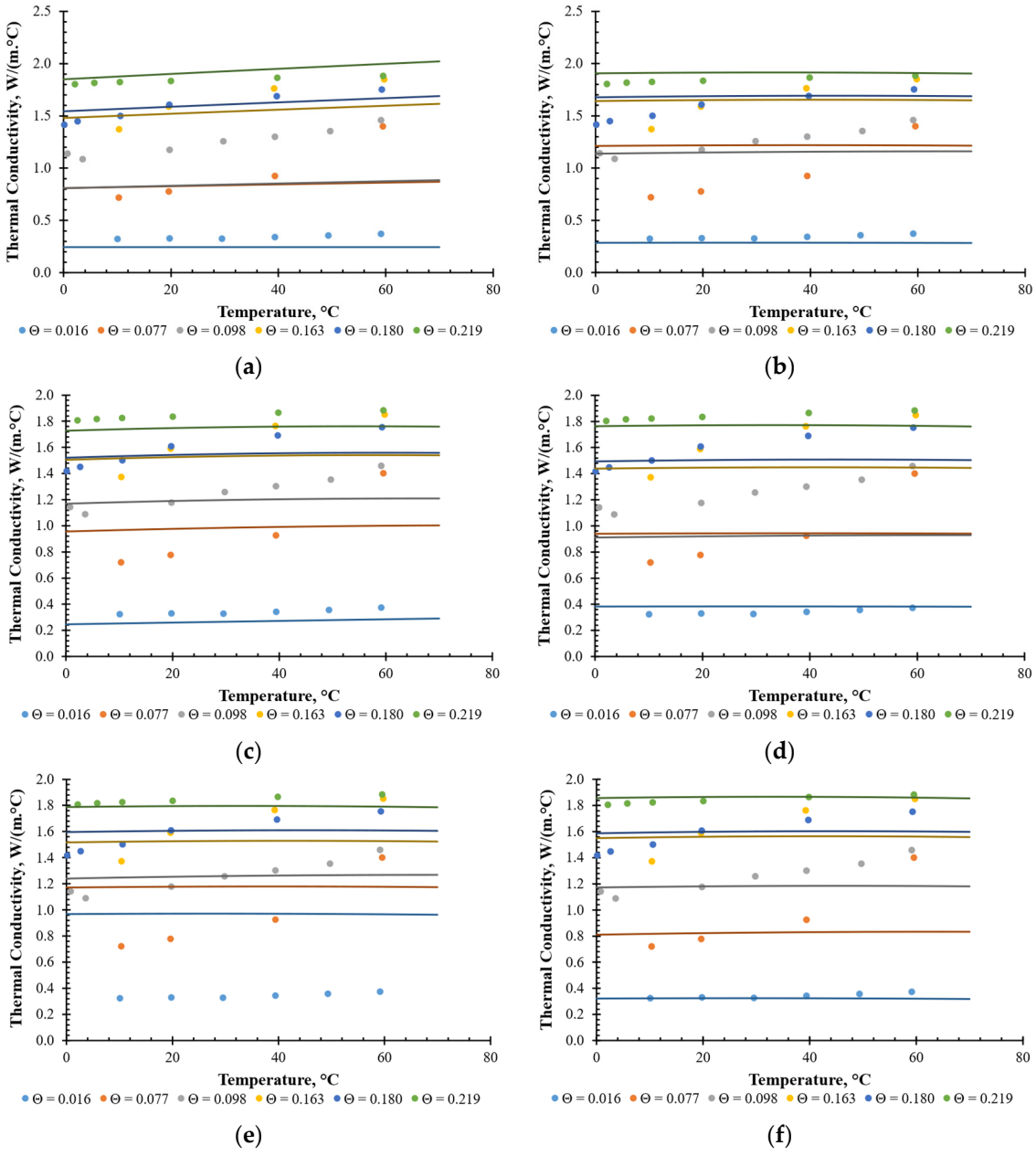


Figure 8. Best fit thermal conductivity models for the Benbrook Sand from the experimental dataset using (**a**) Farouki model; (**b**) Johansen model; (**c**) Campbell et al. model; (**d**) Côté and Konrad model; (**e**) Chen model; and (**f**) Lu et al. model.

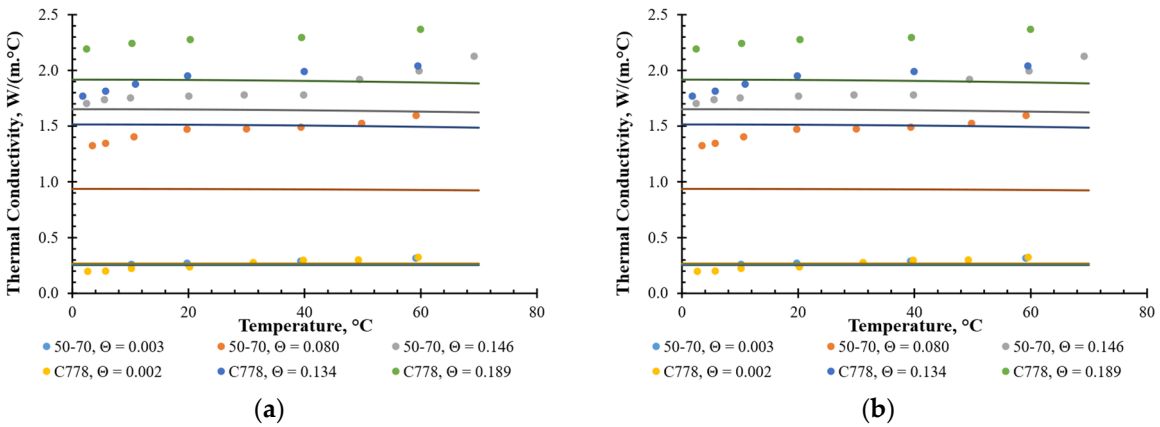


Figure 9. *Cont.*

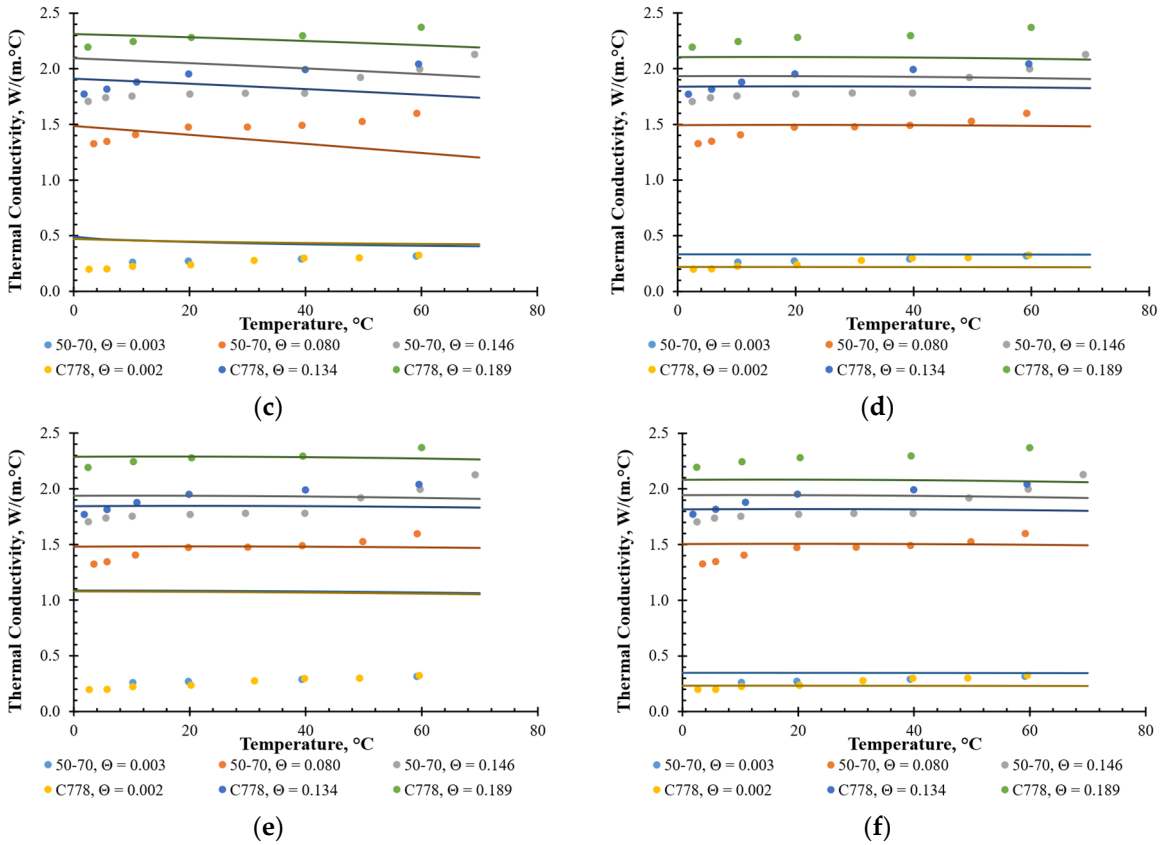


Figure 9. Best fit thermal conductivity models for fine-grained Ottawa sand from the experimental dataset using (**a**) Farouki model; (**b**) Johansen model; (**c**) Campbell et al. model; (**d**) Côté and Konrad model; (**e**) Chen model; and (**f**) Lu et al. model.

The thermal conductivity of the soil at room temperature (λ_{20}) can be approximated closely using the thermal conductivity model from Lu et al. [21], given by Equations (22)–(24). When the change in thermal conductivity due to temperature is added to the thermal conductivity at room temperature (20 °C), the resulting model will closely predict the thermal conductivity at any elevated temperature in unsaturated sands. The combined result, thus, can be presented by Equation (29), which is the proposed thermal conductivity function for modeling at elevated temperatures in unsaturated soils.

$$\lambda_T = \lambda_{20} + \frac{\partial k_{eff}}{\partial T}(T - 20) \quad (29)$$

The proposed model will directly take temperature and saturation into consideration while determining the temperature effect on thermal conductivity, whereas the thermal conductivity at room temperature (λ_{20}) takes mineralogy, porosity, and the thermal conductivity of each phase of soil into consideration. Finally, the above equations can be compiled with Lu et al., and the final form of the model can be presented by Equation (30).

$$\lambda_T = \exp\left(\alpha\left[1 - S^{(\alpha - 1.33)}\right]\right)\left(\lambda_s^{1-n}\lambda_w^n - (-a_1 n + b_1)\right) + (-a_1 n + b_1) + (AS(B - S)\exp(-CS))\cdot(T - 20) \quad (30)$$

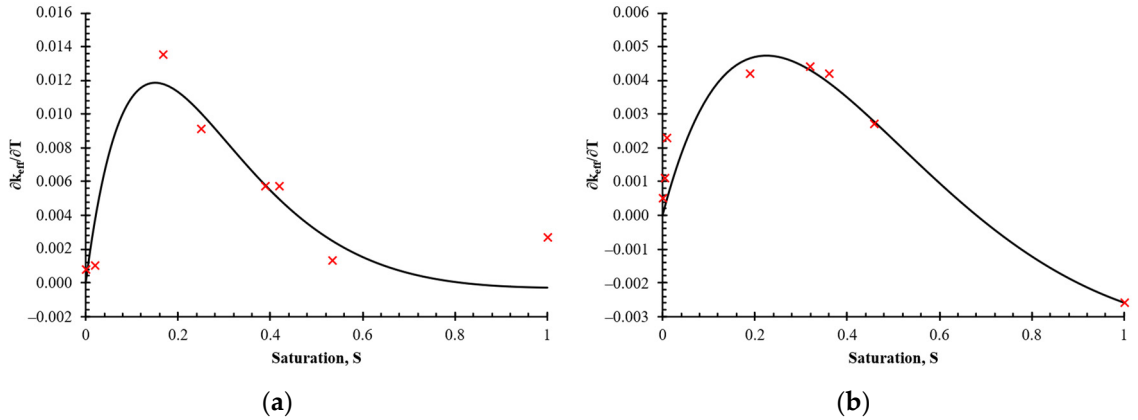
6.4. Model Performance of the Proposed Model

The implementation of the proposed thermal conductivity model began with determining the slope of the best-fit lines from Figure 7 to quantify the temperature effect on thermal conductivity with respect to saturation. To quantify this temperature effect, the unknown temperature dependence at full saturation of the Ottawa and Benbrook sands

was taken based on C109 sand from Tarnawski et al. [38] dataset and silty sand from Nikolaev et al. [39] dataset, respectively. The data were analyzed using Equation (28), and the best-fit parameters were obtained by minimizing the error; these parameters are presented in Table 2. The temperature dependence of thermal conductivity ($\partial k_{eff}/\partial T$) for Benbrook and Ottawa sands is shown in Figure 10. A sharp increase in temperature dependence at low saturation is attributed to the rapid growth of particle contact area and enhanced diffusive heat transfer as the soil wets from a dry condition. At a given moisture content, vapor diffusion increases with temperature and reaches a peak at low to medium saturation levels (0.151 for Benbrook sand and 0.225 for Ottawa sand). Beyond this point, diffusion decreases, reducing temperature sensitivity. Benbrook sand exhibited significantly higher temperature dependence than Ottawa sand, likely due to mineralogical differences. As saturation approaches unity, the absence of air voids limits diffusive heat transfer, and temperature effects are governed primarily by the intrinsic thermal properties of water and solids.

Table 2. The best-fit parameters for the temperature dependence function (Equation (28)).

Parameters	Benbrook Sand	Ottawa Sand
A	0.255	0.0767
B	0.819	0.680
C	5.136	2.249



(**a**) (**b**)

Figure 10. Variation in temperature dependency of thermal conductivity with saturation for (**a**) Benbrook (silty) sand and (**b**) fine-grained Ottawa sands.

The evaluated parameters from Equation (28) were implemented in the proposed model (Equation (30)) to determine the thermal conductivity of the sandy soils at various temperatures and saturation levels. The resulting thermal conductivities predicted by the proposed equation are presented in Figure 11, and the comparison between the measured and best-fit thermal conductivities is shown in Figure 12. These graphs demonstrate the close agreement between the best-fit thermal conductivity values and the experimental results, yielding RMSE values of 0.102 W/(m·°C) and 0.0718 W/(m·°C) for the Benbrook and fine-grained Ottawa sands, respectively. A coefficient of determination (R^2) of 0.978 was obtained from the best-fit data, indicating a very close match with the experimental dataset.

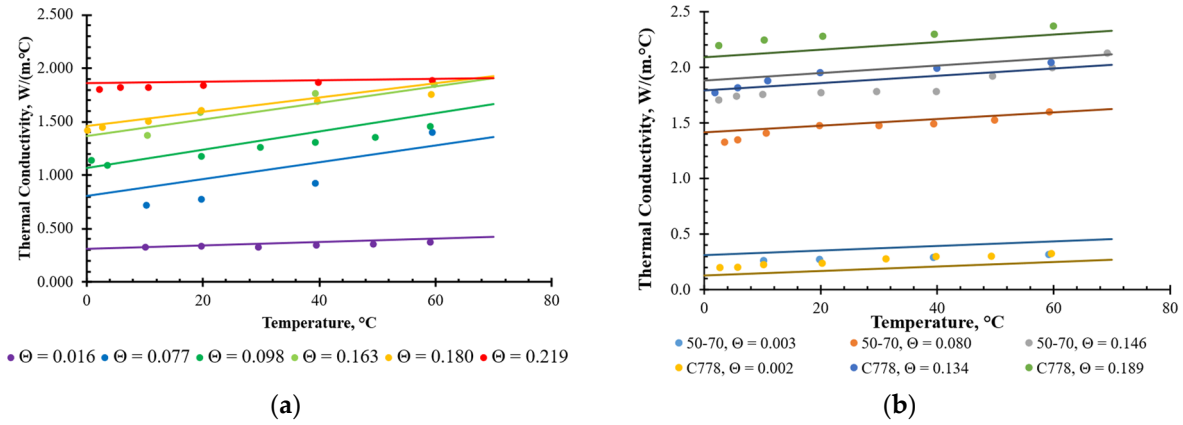


Figure 11. Graphs showing the best-fit predictions from the proposed TCF for (**a**) Benbrook sand and (**b**) Ottawa sand.

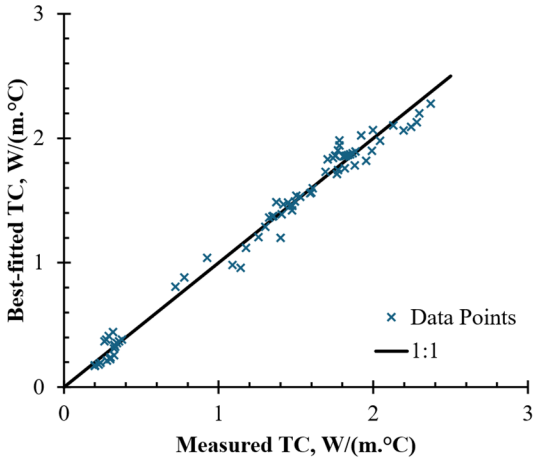


Figure 12. Model performance of the proposed thermal conductivity model based on experimental and best-fit data.

7. Discussion

Most thermal conductivity models for unfrozen soil treat porosity, mineral content, and soil saturation as the dependent variables, although thermal conductivity also depends on temperature. The thermal conductivity models use the volumetric mixing formula, with the thermal conductivities of each phase and porosity as dependent parameters for determining the saturated thermal conductivity (i.e., the upper limit for thermal conductivity), and porosity is used to determine the dry thermal conductivity. The modification factor, Kersten number (K_e), is expressed as a function of saturation and is empirically calibrated based on soil type to account for saturation in the TCFs. Logarithmic [11,24], exponential [21], power law [37], and hyperbolic [25] equations have been recommended by different authors for determining the Kersten number. The thermal conductivity models perform well across a wide range of saturation ratios at room temperature for specific soil types, but they still fail to account for the temperature effect. Modification of De Vries [36] mixing model by Campbell et al. [20] considers temperature as a dependent variable in parameter optimization for equivalent fluid thermal conductivity determination, but still fails to capture the increment in thermal conductivity of the soils due to temperature.

The new model treats the soil's temperature, saturation, porosity, and mineralogy as dependent variables in sandy soils to capture the accurate temperature dependence of thermal conductivity, overcoming the limitations of previously developed models. In this study, the increase in temperature dependency with saturation, followed by a reduction, has been

modeled using an exponential equation that captures the slope of thermal conductivity vs. temperature over the studied temperature range. The addition of a small amount of moisture significantly improves particle contact among soil solids, thereby greatly increasing diffusive heat transfer, leading to a sharp rise in heat transfer and, consequently, in soil thermal conductivity. However, this effect becomes less effective at higher saturations [6]. This phenomenon explains why the temperature dependency increased sharply at low saturation, then gradually decreased beyond 18% saturation.

The proposed model captured the temperature dependence of the thermal conductivity with high accuracy ($RMSE = 0.102\ \mathrm{Wm^{-1}{}^{\circ}C^{-1}}$ and $R^2 = 0.978$) overcoming the past TCFs accuracy while being simple to use. The best performing previous model was Lu et al. ($RMSE = 0.144\ \mathrm{Wm^{-1}{}^{\circ}C^{-1}}$), followed by Côté and Konrad ($RMSE = 0.145\ \mathrm{Wm^{-1}{}^{\circ}C^{-1}}$), Johansen ($RMSE = 0.158\ \mathrm{Wm^{-1}{}^{\circ}C^{-1}}$), Campbell et al. ($RMSE = 0.210\ \mathrm{Wm^{-1}{}^{\circ}C^{-1}}$), Farouki ($RMSE = 0.331\ \mathrm{Wm^{-1}{}^{\circ}C^{-1}}$), and Chen et al. ($RMSE = 0.394\ \mathrm{Wm^{-1}{}^{\circ}C^{-1}}$). This shows that the proposed thermal conductivity model can estimate soil thermal conductivity with higher accuracy.

8. Conclusions

In this study, a new TCF was introduced by advancing the work of Lu et al. [21] model to introduce the temperature dependence of the thermal conductivity in 0 °C to 70 °C temperature range in sandy soils. Several experiments were conducted in a heating cell to determine thermal conductivity at varying saturation levels and temperatures using the steady-state method, while keeping porosity as constant as possible. The performance of the proposed thermal conductivity model was compared with several previously developed, well-accepted models. The proposed TCF captured the temperature dependence of thermal conductivity, which past thermal conductivity models have poorly modeled. The newly developed TCF can be used to simulate truly coupled heat and moisture transfer in soils and to model geothermal processes in thawed soils, where temperature can play an important role. Furthermore, the model can be extended to different soil types by fitting it to experimental data from lab tests.

Author Contributions: Conceptualization, A.P., X.Y. and L.R.H.; methodology, X.Y. and A.P.; validation, A.P.; formal analysis, A.P., X.Y. and L.R.H.; investigation, A.P. and X.Y.; resources, X.Y. and L.R.H.; data curation, A.P. and X.Y.; writing—original draft preparation, A.P.; writing—review and editing, X.Y. and L.R.H.; visualization, A.P. and X.Y.; supervision, L.R.H. and X.Y.; project administration, X.Y. and A.P.; funding acquisition, X.Y. All authors have read and agreed to the published version of the manuscript.

Funding: The funding support from the University of Texas at Arlington to A. Pokhrel is acknowledged.

Data Availability Statement: Data supporting the findings of this research are present within the text.

Conflicts of Interest: The authors declare no conflicts of interest.

References

1. Haque, M.A.; Ku, S.; Haruna, S.I. Soil thermal properties: Influence of no-till cover crops. *Can. J. Soil Sci.* **2024**, *104*, 246–256. [CrossRef]
2. Firat, M.E.O. Experimental investigation on the thermal characteristics and grey correlation analysis of frost penetration depths for different subgrade soils. *Environ. Earth Sci.* **2021**, *80*, 394. [CrossRef]
3. Kaneza, N.; Pokhrel, A.; Hoyos, L.R.; Yu, X. Thermally Induced Moisture Flow in a Silty Sand under a 1-D Thermal Gradient. *Geosciences* **2024**, *14*, 207. [CrossRef]
4. Deshmukh, A.; Puppala, A.J.; Bhaskar, P.; Yu, X.; Fakhrabadi, A.; Lei, G. Design and Performance of a Shallow Geothermal Energy–Supplemented Bridge Deicing System on an In-Service Bridge in North Texas. *J. Geotech. Geoenviron. Eng.* **2025**, *151*, 05025004. [CrossRef]

5. Honeycutt, C. Soil Freeze-Thaw Processes: Implications for Nutrient Cycling. *J. Minn. Acad. Sci.* **1995**, *59*, 9–14.
6. Philip, J.; De Vries, D.A. Moister Movement in Porous Materials under Temperature Gradients. *Trans. Am. Geophys. Union* **1957**, *38*, 2–22.
7. De Vries, D.A. Thermal properties of soils. In *Physics of Plant Environment*; North-Holland Publishing Company: Amsterdam, The Netherlands, 1963; pp. 210–235.
8. Ren, T.; Noborio, K.; Horton, R. Measuring soil water content, electrical conductivity, and thermal properties with a thermos—Time domain reflectometry probe. *Soil Sci. Soc. Am. J.* **1999**, *63*, 450–457. [CrossRef]
9. Shiozawa, S.; Campbell, G.S. Soil thermal conductivity. *Remote Sens. Rev.* **1990**, *5*, 301–310. [CrossRef]
10. Bristow, K.; White, R.; Kluitenberg, G. Comparison of single and dual probes for measuring soil thermal properties with transient heating. *Soil Res.* **1994**, *32*, 447–464. [CrossRef]
11. Farouki, O.T. *Thermal Properties of Soils*; U.S. Army Corps of Engineers, Cold Regions Research and Engineering Laboratory: Hanover, NH, USA, 1981.
12. Alrtimi, A.; Rouainia, M.; Haigh, S. Thermal conductivity of a sandy soil. *Appl. Therm. Eng.* **2016**, *106*, 551–560. [CrossRef]
13. Alrtimi, A.; Rouainia, M.; Manning, D.A.C. An improved steady-state apparatus for measuring thermal conductivity of soils. *Int. J. Heat Mass Transf.* **2014**, *72*, 630–636. [CrossRef]
14. Kim, D.; Oh, S. Measurement and comparison of thermal conductivity of porous materials using box, dual-needle, and single-needle probe methods—A case study. *Int. Commun. Heat Mass Transf.* **2020**, *118*, 104815. [CrossRef]
15. Zhu, J. A new analytical thermal conductivity model for three-phase porous materials. *Therm. Adv.* **2025**, *4*, 100069. [CrossRef]
16. Wu, Y.-H.; Wu, Y.-F.; Fan, L.-W.; Yu, Z.-T.; Khodadadi, J.M. Thermal conductivity of soil: A review on the vast experimental data and predictive models. *Int. J. Therm. Sci.* **2025**, *208*, 109486. [CrossRef]
17. He, H.; He, D.; Jin, J.; Smits, K.M.; Dyck, M.; Wu, Q.; Si, B.; Lv, J. Room for improvement: A review and evaluation of 24 soil thermal conductivity parameterization schemes commonly used in land-surface, hydrological, and soil-vegetation-atmosphere transfer models. *Earth-Sci. Rev.* **2020**, *211*, 103419. [CrossRef]
18. Chen, T.; Fei, W.; Narsilio, G.A. Effective thermal conductivity of granular soils: A review of influencing factors and prediction models towards an investigation framework through multiscale characters. *Can. Geotech. J.* **2025**, *62*, 1–17. [CrossRef]
19. Kersten, M.S. *Thermal Properties of Soils*; University of Minnesota: Minneapolis, MN, USA, 1949.
20. Campbell, G.; Jungbauer, J., Jr.; Bidlake, W.; Hungerford, R. Predicting the effect of temperature on soil thermal conductivity. *Soil Sci.* **1994**, *158*, 307–313. [CrossRef]
21. Lu, S.; Ren, T.; Gong, Y.; Horton, R. An Improved Model for Predicting Soil Thermal Conductivity from Water Content at Room Temperature. *Soil Sci. Soc. Am. J.* **2007**, *71*, 8–14. [CrossRef]
22. Wang, H.; Li, D.; Xia, M.; Li, X. Study on thermal conductivity of improved soil under different freezing temperatures. *PLoS ONE* **2023**, *18*, e0292560. [CrossRef]
23. Tarnawski, V.R.; Leong, W.H.; McCombie, M.; Bovesecchi, G. Estimating Soil Thermal Conductivity by Weighted Average Models with Soil Solids as a Continuous Medium. *Int. J. Thermophys.* **2022**, *43*, 182. [CrossRef]
24. Johansen, O. *Thermal Conductivity of Soils*; Cold Regions Research and Engineering Laboratory: Hanover, NH, USA, 1977; p. 322.
25. Côté, J.; Konrad, J.-M. A generalized thermal conductivity model for soils and construction materials. *Can. Geotech. J.* **2005**, *42*, 443–458. [CrossRef]
26. Liu, F.; Luo, H.; Luo, J.; Wan, X. Establishment and Verification of a Thermal Conductivity Model for Fine-Grained Soils. *J. Cold Reg. Eng.* **2026**, *40*, 04025046. [CrossRef]
27. Bi, J.; Zhang, M.; Chen, W.; Lu, J.; Lai, Y. A new model to determine the thermal conductivity of fine-grained soils. *Int. J. Heat Mass Transf.* **2018**, *123*, 407–417. [CrossRef]
28. Cao, T.D.; Thota, S.K.; Vahedifard, F.; Amirlatifi, A. General Thermal Conductivity Function for Unsaturated Soils Considering Effects of Water Content, Temperature, and Confining Pressure. *J. Geotech. Geoenviron. Eng.* **2021**, *147*, 04021123. [CrossRef]
29. Ji, H.; Fu, X.; Nan, Z.; Zhao, S. An effective medium theory-based unified model for estimating thermal conductivity of unfrozen and frozen soils. *CATENA* **2024**, *239*, 107942. [CrossRef]
30. Ghanbarian, B.; Daigle, H. Thermal conductivity in porous media: Percolation-based effective-medium approximation. *Water Resour. Res.* **2016**, *52*, 295–314. [CrossRef]
31. Bang, H.-T.; Yoon, S.; Jeon, H. Application of machine learning methods to predict a thermal conductivity model for compacted bentonite. *Ann. Nucl. Energy* **2020**, *142*, 107395. [CrossRef]
32. Li, K.-Q.; Liu, Y.; Kang, Q. Estimating the thermal conductivity of soils using six machine learning algorithms. *Int. Commun. Heat Mass Transf.* **2022**, *136*, 106139. [CrossRef]
33. United States Department of Commerce; National Bureau of Standards; Powell, R. *Thermal Conductivity of Selected Materials*; U.S. Government Printing Office: Washington, DC, USA, 1966; Volume 8.
34. Midttømme, K.; Roaldset, E.; Aagaard, P. Thermal conductivity of selected claystones and mudstones from England. *Clay Miner.* **1998**, *33*, 131–145. [CrossRef]

35. Thermal Conductivity of Water: Temperature and Pressure Data. Available online: https://www.engineeringtoolbox.com/water-liquid-gas-thermal-conductivity-temperature-pressure-d_2012.html (accessed on 10 December 2025).
36. De Vries, D.A. Thermal Conductivity of Soil. *Nature* **1956**, *178*, 1074. [CrossRef]
37. Chen, S.X. Thermal conductivity of sands. *Heat Mass Transf.* **2008**, *44*, 1241–1246. [CrossRef]
38. Tarnawski, V.R.; Momose, T.; Leong, W.H. Thermal Conductivity of Standard Sands II. Saturated Conditions. *Int. J. Thermophys.* **2011**, *32*, 984–1005. [CrossRef]
39. Nikolaev, I.V.; Leong, W.H.; Rosen, M.A. Experimental Investigation of Soil Thermal Conductivity Over a Wide Temperature Range. *Int. J. Thermophys.* **2013**, *34*, 1110–1129. [CrossRef]

Disclaimer/Publisher's Note: The statements, opinions and data contained in all publications are solely those of the individual author(s) and contributor(s) and not of MDPI and/or the editor(s). MDPI and/or the editor(s) disclaim responsibility for any injury to people or property resulting from any ideas, methods, instructions or products referred to in the content.